LiBC – Synthesis, Electrochemical and Solid-state NMR Investigations

Thorsten Langer[a,b], Sven Dupke[b], Christian Dippel[b], Martin Winter[b], Hellmut Eckert[b], and Rainer Pöttgen[a]

[a] Institut für Anorganische und Analytische Chemie, Universität Münster, Corrensstraße 30, D-48149 Münster, Germany

[b] Institut für Physikalische Chemie, Universität Münster, Corrensstraße 30, D-48149 Münster, Germany

Reprint requests to R. Pöttgen. E-mail: pottgen@uni-muenster.de

Z. Naturforsch. **2012**, *67b*, 1212 – 1220 / DOI: 10.5560/ZNB.2012-0223
Received August 20, 2012

LiBC was synthesized from the elements in a sealed niobium ampoule. It represents a totally intercalated heterographite with a structural relationship to graphite, the most commonly used anode material for lithium ion batteries. Since LiBC could accommodate three times as much lithium as graphite, its electrochemical properties in the anode and the cathode voltage range were investigated. However, LiBC did show poor performance both as an anode and as a cathode material. The unfavorable characteristics of LiBC with respect to electrochemical de-lithiation and re-insertion can be rationalized on the basis of nuclear magnetic resonance results. ^{7}Li and ^{6}Li isotropic chemical shifts are consistent with complete ionization of the lithium species. Variable-temperature static ^{7}Li NMR lineshapes indicate that the mobility of the lithium ions is rather restricted, even at temperatures up to 500 K. The ^{11}B and ^{13}C NMR parameters are consistent with those measured in sp^2-hybridized boron/carbon networks and also support the ionic bonding model.

Key words: Lithium, Heterographite, Solid-state NMR, Electrochemical Properties

Introduction

High capacity electrode materials are crucial for the development of high-energy lithium ion batteries. Therefore the discovery of novel anode and cathode materials is an important task in material science [1 – 3]. The most commonly used anode material in commercial lithium ion batteries is graphite [4 – 7] which has a theoretical capacity of 372 mA h g^{-1} resulting in the final fully lithiated phase LiC_6 [8, 9].

The borocarbide LiBC represents a totally intercalated heterographite and was first reported by Wörle *et al*. in 1995 [10]. Recently, it has attracted a lot of interest since it is isoelectronic with the 39 K superconductor MgB_2 [11] and adopts a similar hexagonal structure with alternating boron-carbon and lithium layers. Theoretical studies have predicted superconductivity for hole-doped $Li_{1-x}BC$ with a T_C up to twice as high as that of MgB_2 [12]. As a result, Li_xBC compounds were synthesized by many groups in bulk quantities [13 – 20], and their electronic and optical properties were investigated [21, 22]. However, synthesized samples of $Li_{1-x}BC$ did not show superconductivity [13, 14]. It is remarkable that lithium-deficient LiBC could be obtained up to a composition of $Li_{0.38}BC$ using thermal synthesis methods [12], even though earlier results suggest that Li_xBC is only stable for $x > 0.5$ [18, 20], and a phase transition occurs at lower lithium content [16]. This finding suggests that LiBC might be a promising active material for lithium ion batteries, in particular as its structure is also related to that of LiC_6. The boron and carbon atoms build up layers of condensed six-membered rings, and the lithium atoms are located in between these layers. If electrochemical lithiation and delithiation of LiBC would be possible in the range $LiBC \leftrightarrow Li_{0.38}BC + 0.62\,Li$, a theoretical capacity of 728 mA h g^{-1} could be achieved, more than twice as high as that of LiC_6.

This article deals with the synthesis, and the structural, $^{6/7}$Li and ^{11}B solid-state NMR, and electrochemical characterization of LiBC. Because of the close structural resemblance of LiBC and LiC_6, we first tested the suitability of this compound for an-

ode applications. Recently, Xu *et al*. published a first-principle study of LiBC as a cathode material [23]. They predicted an equilibrium lithium insertion potential of 2.3 – 2.4 V (*vs*. Li/Li^+) and a reversible electrochemical reaction LiBC $\leftrightarrow$ $Li_{0.5}BC + 0.5\,Li$. This would correspond to a theoretical capacity of 587 mA h g^{-1}. Because of the relatively positive insertion potential, the material was also tested for cathode material applications.

Experimental

Synthesis

Starting materials for the synthesis of LiBC were lithium rods (Merck, > 99.5 %), boron lumps (Aldrich, > 99.9 %) and carbon flakes (Aldrich, > 99.9 %). The lithium rods were cut into smaller pieces under dry paraffin oil and subsequently washed with *n*-hexane. The lithium pieces were kept in Schlenk tubes under argon prior to the reaction. Argon was purified with titanium sponge (900 K), silica gel, and molecular sieves. The lithium pieces were mixed with the boron lumps and the carbon flakes in an atomic ratio of 3 : 1 : 1 under flowing argon and then arc-welded in a niobium ampoule under an argon pressure of about 700 mbar. The niobium tube was then placed in the water-cooled sample chamber of an induction furnace [24]. The sample was rapidly heated to 1800 K and held at that temperature for 15 min. Subsequently, the sample was cooled to 1000 K within 10 min and kept at that temperature for another 2 h before it was quenched by switching off the furnace. The sample could readily be separated from the tube, and no reaction with the container material was observed. The excess of lithium was removed with ethanol (> 99 %). Both single crystals and ground powder of LiBC show golden metallic luster.

X-Ray diffraction

The polycrystalline LiBC sample was characterized by powder X-ray diffraction on a Bruker D8 Advance diffractometer using Cu K_α radiation. The hexagonal lattice parameters (see Table 1) were deduced from a least-squares fit of the powder diffraction data. Correct indexing of the diffraction lines was ensured by an intensity calculation using the positional parameters obtained from the structure refinement. The lattice parameters agree well with the data given by Wörle *et al*. of $a = 275.23(3)$ and $c = 705.8(2)$ pm [10]. Owing to preferred orientation effects of the hexagonal platelets, the reflection intensity distribution was found to deviate from the theoretically calculated one.

Well shaped single-crystalline golden hexagonal plates of LiBC were obtained by mechanical fragmentation of the regulus prepared by high-frequency annealing. These crystals were glued to quartz fibers using bees wax. Their quality for intensity data collection was checked by Laue photographs on a Buerger camera (white Mo radiation, image plate technique, Fuji-film BAS-1800). A suitable crystal was measured at room temperature on a Stoe IPDS-II diffractometer (graphite-monochromatized Mo K_α radiation, oscillation mode). All relevant crystallographic data and details of the data collection are listed in Table 1.

Table 1. Crystallographic data and structure refinement of LiBC.

Empirical formula	LiBC
Molar mass, g mol^{-1}	29.76
Crystal size, μm^3	$10 \times 80 \times 80$
Space group; Z	$P6_3/mmc$; 2
Structure type	ZrBeSi
Lattice parameters (powder data)	
a, pm	274.9(1)
c, pm	705.3(1)
Cell volume V, nm^3	0.0462(1)
Calculated density, g cm^{-3}	2.14
$F(000)$, e	28
Diffractometer	IPDS-II
Radiation; λ, pm	Mo K_α; 71.073
Absorption coefficient, mm^{-1}	0.1
θ range, deg	5 – 35
hkl range	±4; ±4; ±10
Total no. reflections	641
Independent reflections/R_{int}	54/0.0583
Reflections with $I > 2\sigma(I)/R_\sigma$	41/0.0223
Data/ref. parameters	54/7
$R1/wR2$ for $I > 2\sigma(I)$	0.0428/0.1026
$R1/wR2$ for all data	0.0554/0.1080
Goodness-of-fit (F^2)	1.333
Largest diff. peak/hole, e $Å^{-3}$	0.31/ – 0.21

Electrochemical investigations

For electrochemical characterization the sample was ground to a fine powder in an agate mortar. The powder was mixed with carbon black C65 (Timcal) and a 5 wt.-% solution of PVdF in NMP (LiBC : SuperP : PVdF mass ratio of 80 : 10 : 10.). Subsequently, the mixture was homogenized for 30 min using an Ultra-Turaxx at 5000 rpm (anode) and a ballmill (Fritsch Pulverisette 4) at 250 rpm. The slurry was applied to a dendritic copper and alumina foil, respectively, with a wet-film thickness of 100 μm using a doctor blade and dried at 60 °C for 12 h.

Subsequently, disc-shaped electrodes with a diameter of 1.2 cm were cut from the cast copper and aluminum foil, respectively. The electrodes were dried for 12 h in a Büchi vacuum oven at 10^{-3} mbar and 120 °C. For electrochemical characterization three electrode Swagelok cells were assembled in an argon-filled glovebox (H_2O, O_2 content < 0.1 ppm) with lithium metal as the counter and reference

electrode material and a 1 M solution of $LiPF_6$ in EC : DEC 3 : 7 (wt.-%) as the electrolyte for the anode tests and a 1 M solution of $LiBF_4$ in EC : DMC 1 : 1 as the electrolyte for the cathode tests. The cells were connected to a Basytec battery test system and cycled under potential control.

Solid-state NMR spectroscopy

^{7}Li NMR experiments were conducted on a Bruker Avance DSX 500 spectrometer interfaced with a 4.7 T magnet. Variable-temperature static ^{7}Li NMR spectra were measured at 77.77 MHz using commercial static 5 mm and commercial WVT-MAS probes, respectively. Spectra were acquired using a $90°_x$–τ–$90°_y$ solid echo sequence utilizing a 90° pulse length of 4 μs, an interpulse delay t of 30 μs and a relaxation delay of 20 s. Dry nitrogen gas was used for cooling, and the temperature was calibrated using the ^{207}Pb resonance of $Pb(NO_3)_2$ [25]. $^{6/7}$Li and ^{11}B MAS-NMR spectra were measured at a spinning speed of 24.0 kHz on a Bruker Avance DSX 400 (9.4 T) spectrometer, while ^{13}C MAS-NMR was measured on a Bruker Avance III spectrometer (7.04 T) at a spinning speed of 12.0 kHz. 90° pulse lengths were on the order of 4 – 8 μs, and relaxation delays of 20 s (^{7}Li), 10 s (^{13}C), 30 s (^{11}B) and 250 s (^{6}Li) were used. An aqueous 1 M LiCl solution, BF_3 etherate and TMS were used as references for $^{6/7}$Li, ^{11}B and ^{13}C NMR measurements, respectively. Lineshapes were deconvoluted using the DMFIT software package [26] as either superpositions of Gauss/Lorentz lineshapes or as second-order quadrupolar lineshapes.

Results and Discussion

Structure refinement

Careful analysis of the LiBC data set showed a primitive hexagonal lattice, and the systematic extinctions were compatible with space group $P6_3/mmc$. The atomic parameters of LiBC known from the literature [20] were taken as starting values, and the structure was refined with anisotropic displacement parameters for the boron and carbon atoms with SHELXL-97 (full-matrix least-squares on F_o^2) [27]. The lithium site was refined isotropically. The refinement proceeded smoothly to the residuals listed in Table 1. The final difference electron density synthesis was flat. The positional parameters are listed in Table 2.

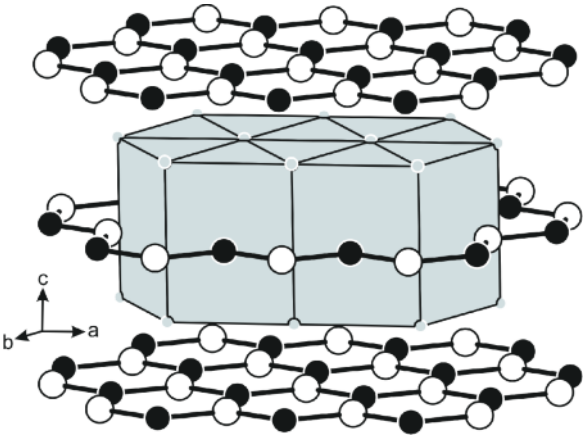

Fig. 1. Crystal structure of LiBC; view approximately along the crystallographic *b* axis. Lithium, boron and carbon atoms are drawn as gray, open and black circles, respectively. The trigonal prismatic coordination of the boron and carbon atoms is emphasized.

Further details of the crystal structure investigation may be obtained from Fachinformationszentrum Karlsruhe, 76344 Eggenstein-Leopoldshafen, Germany (fax: +49-7247-808-666; E-mail: crysdata@fiz-karlsruhe.de, http://www.fiz-karlsruhe.de/request_for_deposited_data.html) on quoting the deposition number CSD-425059.

Crystal chemistry

LiBC crystallizes with the hexagonal ZrBeSi-type structure [28], space group $P6_3/mmc$, a superstructure of the AlB_2-type structure [29], see Fig. 1. The lithium atoms build up a primitive hexagonal packing of trigonal prisms whose centers are alternately occupied by boron and carbon atoms. The latter build up planar layers of condensed six-membered rings in which the boron atoms have only carbon neighbors and *vice*

Table 2. Atomic coordinates and anisotropic displacement parameters (pm^2) for LiBC. U_{eq} is defined as one third of the trace of the orthogonalized U_{ij} tensor. $U_{11} = U_{22}$; $U_{13} = U_{23} = 0$.

Atom	Wyckoff-Position	x	y	z	U_{11}	U_{33}	U_{12}	U_{eq}/U_{iso}
Li	2*a*	0	0	0				153(12)
B	2*d*	1/3	2/3	3/4	86(10)	111(22)	43(5)	95(9)
C	2*c*	1/3	2/3	1/4	61(9)	106(19)	31(5)	76(9)

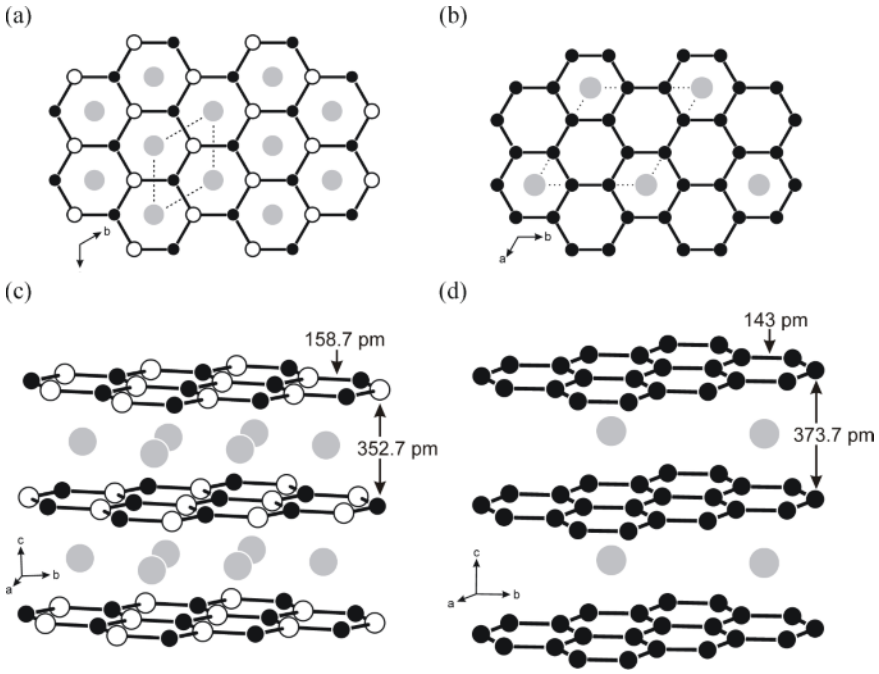

Fig. 2. Projection of the LiBC (a) and LiC_6 (b) structure along the crystallographic *c* axis. The unit cell is indicated by dashed lines. Views of the LiBC (c) and LiC_6 (d) structures approximately along the *a* axis. Some relevant interatomic distances are given. Lithium, boron and carbon atoms are drawn as gray, open and black circles, respectively.

versa. The layers are stacked in an AB sequence along the *c* axis. This causes a doubling of the crystallographic *c* translation as compared to AlB_2.

The B–C distances (158.7 pm) are slightly shorter than the sum of covalent radii (165 pm) and thus indicate strong bonding within the BC layers. The Li–B and Li–C distances are identical (237.2 pm), and both are significantly longer than the sum of covalent radii (Li + B = 211 pm; Li + C = 200 pm [30]). A more detailed structure discussion of LiBC is available in the literature [10].

Fig. 2 shows the structures of both LiBC and LiC_6 (space group *P6/mmm*) in order to depict the structural similarity of these compounds. The carbon and the alternating carbon and boron atoms, respectively, build layers in the crystallographic *ab* plane which are stacked along the *c* axis. The interatomic distances within these layers are somewhat larger in LiBC (158.7 pm) than in LiC_6 (143 pm) [31], whereas the distances between the layers are smaller for LiBC (352.7 pm) than for LiC_6 (373.7 pm). The carbon and boron atoms build up hexagonal prisms in between the layers. In LiBC a lithium atom is located in each of these prisms whereas in LiC_6 only every third prism is occupied by a lithium atom. Hence, if reversible electrochemical lithiation and delithiation would be possible into/from LiBC, up to three times as much lithium could be stored in LiBC than in LiC_6.

Electrochemistry

The suitability of LiBC as an anode and cathode material in lithium ion batteries, respectively, was investigated by cyclic voltammetry.

The applicability of LiBC as an anode material was checked by means of voltammetry within the potential range from 0.1 to 2.2 V *vs.* Li/Li^+ at a sweep rate of 50 $\mu V\,s^{-1}$. The current *vs.* potential plot is presented in Fig. 3a. The corresponding capacities, obtained by integration of the cathodic and anodic peaks, are given in Table 3. Since the open circuit potential (OCP) of LiBC was determined to be 2.7 V *vs.* Li/Li^+, the experiment was started at OCP with ramping the potential down to 0.1 V. However, LiBC did not show any significant de-intercalation processes, indicating an irreversible lithium uptake. The observed charge and discharge capacities are caused by reversible lithiation of the conductive agent carbon black (C65) as well as by electrolyte decomposition [32–34] and solid electrolyte interphase (SEI) [35–37] formation on the surfaces of all electronically conductive electrode components in the first discharge. In summary, LiBC is

Potential range (V)	0.1 – 2.5					1.5 – 4.8				
Cycle	1	2	3	4	5	1	2	3	4	5
Charge capacity	4.34	6.14	6.45	6.68	6.77	132.6	64.8	54.8	42.4	37.1
Discharge capacity	14.89	5.88	5.33	5.07	4.63	35.8	36.3	32	30.5	27.5

Table 3. Specific capacities (mA h g^{-1}) for LiBC in the potential ranges 0.1 – 2.5 V and 1.5 – 4.8 V in the first five cycles obtained by cyclic voltammetry.

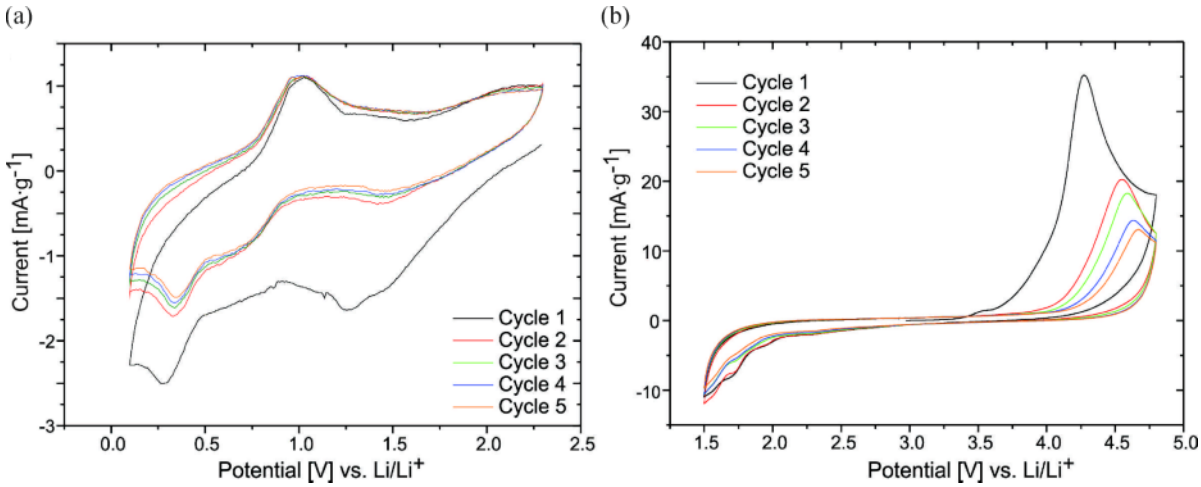

Fig. 3. Cyclic voltammetry of LiBC in a potential range of 0.1 – 2.2 V (a) and 1.5 – 4.8 V (b) *vs.* Li/Li^+.

not applicable as an anode material in lithium ion batteries since no reversible lithium intercalation can be achieved. The current *vs.* potential curve for LiBC tested in the cathode potential range (1.5 – 4.8 V *vs.* Li/Li^+) is shown in Fig. 3b. The corresponding capacities are listed in Table 3. In the anodic curve an oxidation peak with a maximum at 4.3 V *vs.* Li/Li^+ is detected which fades and shifts to higher potentials with increasing cycle count which could be caused by an increasing cell resistance. In the cathodic curve a reduction peak with an onset potential of about 2 V *vs.* Li/Li^+ is detected. In the cyclic voltammogram in the potential range of 0.1 – 2.2 V *vs.* Li/Li (Fig. 3 a) no such process is detected. Hence, one can assume that the oxidation and reduction peak of the cyclic voltammogramm in the 1.5 – 4.8 V region *vs.* Li/Li^+ (Fig. 3b) might be attributed to lithium extraction and insertion, respectively. The current peaks at above 4.5 V could also be related to anion intercalation processes [38 – 40] of the lithium salt anions, in this case BF_4^- anions. Since no real maximum was detected for the reduction peak we conclude that on the time scale of the voltammetric experiment, lithium insertion was not fully completed when reaching the lower potential limit of 1.5 V. A look at the capacities obtained during charge and discharge (Table 3) reveals a maximum charge capacity of 132.6 mA h g^{-1} (1st cycle) that fades to 37.1 mA h g^{-1} in the 5th cycle. These values correspond to compositions of $Li_{0.89}BC$ and $Li_{0.97}BC$, respectively, after delithiation.

Compared to the predictions from first principle calculations by Xu *et al.* [23] who calculated a lithium intercalation potential of 2.3 – 2.4 V *vs.* Li/Li^+, the experimentally determined one is significantly lower (< 1.5 V *vs.* Li/Li^+).

$^{6/7}$Li, ^{11}B and ^{13}C solid-state NMR spectroscopy

The ^{7}Li MAS-NMR spectrum of LiBC at room temperature is presented in Fig. 4. A single resonance is detected at − 1.3 ppm *vs.* 1 M aqueous LiCl solution. The considerable width of this line (full width at half maximum FWHM = 1260 Hz) can be attributed to residual homonuclear ^{7}Li-^{7}Li dipolar couplings which cannot be fully averaged out by MAS. Furthermore, the signal is flanked by spinning sidebands, which arise from the influence of MAS upon the $m = 1/2 \leftrightarrow m = 3/2$ "satellite transitions" that are anisotropically broadened by nuclear electric quadrupolar interactions. In contrast, the ^{6}Li MAS-NMR spectrum is considerably simpler. Because of the smaller magnetic moment and the lower natural abundance of the ^{6}Li isotope the homonuclear ^{6}Li-^{6}Li dipolar interactions are much weaker in this case, resulting in a much sharper

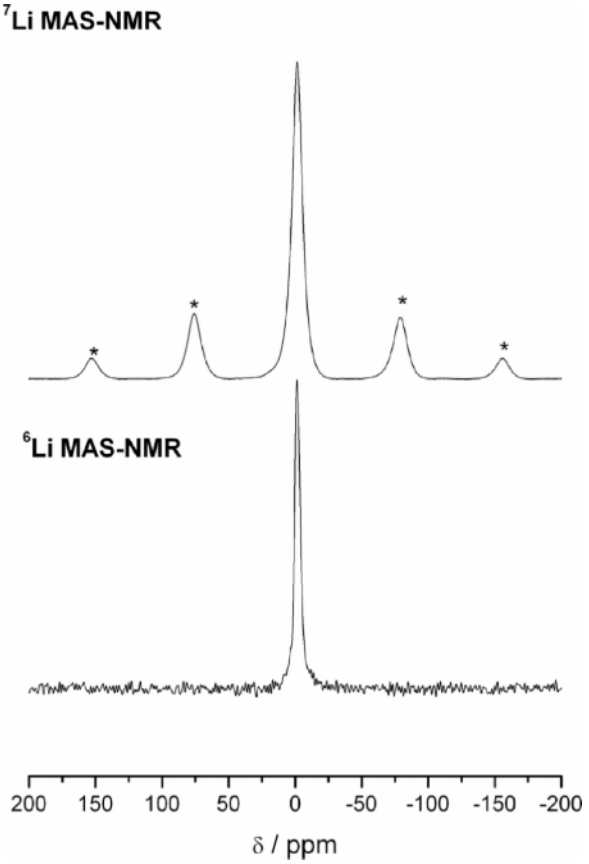

Fig. 4. ^{6}Li and ^{7}Li MAS-NMR at room temperature and spinning speeds of 12 kHz. Spinning sidebands are marked by asterisks.

MAS NMR signal (FWHM = 278 Hz); in addition no spinning sideband patterns appear, as the anisotropic broadening effect of the static ^{6}Li spectrum by first-order quadrupolar perturbations is very small. The resonance shifts of the $^{6/7}$Li NMR signals indicate that the lithium atoms are fully ionized, and that the electron is completely transferred to the BC layers. Hence, the electronic situation in this compound is best described by the formulation $Li^+[BC]^-$, indicating that the structure will become unstable upon lithium extraction.

The room-temperature static ^{7}Li NMR spectrum (Fig. 5a) can be deconvoluted into two components: a broad major signal (FWHM = 13.8 kHz) and a sharp minor signal ($\sim$ 2 %, FWHM = 0.8 kHz). The large width of the major signal arises from the strong broadening effects of homonuclear ^{7}Li-^{7}Li dipole-dipole interactions. In addition, quadrupole-broadened satellite transitions are apparent in the wings of the spectrum. The sharp ^{7}Li NMR signal belongs to a mobile lithium species having a motional correlation time τ that is short compared to the inverse ^{7}Li NMR linewidth, *i. e.* $\tau < 0.1$ ms. We attribute this species to some lithium atoms that are located in the vicinity of structural defects and thus have higher mobility. Fig. 5b summarizes the results of temperature-dependent measurements. While unambigous deconvolution of these spectra is not possible as both the central transition and the quadrupole-broadened satellite transitions are inseparably superimposed in the broad component, the fraction of mobile lithium can be estimated from simple integration of the area comprised by the sharp peak. Fig. 5c shows that this fraction increases gradually with increasing temperature, consistent with a behavior typically observed for a large dynamic heterogeneity, *i. e.* a wide distribution of correlation times. Owing to the integration procedure and the rather ill-defined lineshape of the broad component the actual fraction of mobile lithium may be subject to considerable error. Still it appears that up to 500 K, a majority of the lithium atoms have rather restricted mobility.

The NMR results discussed above regarding both structure and mobility of the lithium ions in LiBC are consistent with the low degree of lithium extractability seen in the electrochemical studies. The lithium atoms are fully ionized and held within the structure rather tightly by strong Coulombic interactions. The situation is fundamentally different from that in LiC_6 where Li can be reversibly removed and re-inserted at room temperature. For the latter compound the NMR spectra reveal considerable electron density on the lithium species, as reflected by a resonance shift of 44 ppm [41 – 43]. In addition, variable-temperature ^{7}Li static and MAS-NMR studies have shown that the lithium atoms in LiC_6 have considerable mobility at room temperature [41 – 43], enhancing electrochemical intercalation and de-intercalation kinetics.

Fig. 6a shows the ^{11}B MAS-NMR spectrum of LiBC at room temperature. The resonance with an isotropic chemical shift of 49 ppm reflects the central $1/2 \leftrightarrow -1/2$ transition, which is affected by second-order quadrupolar perturbations and characterized by a quadrupolar coupling constant $C_Q = 2.80 \pm 0.05$ MHz and an electric field asymmetry parameter $\eta_Q = 0.1 \pm 0.1$. These lineshape parameters are close to those measured for boron dopants in graphite

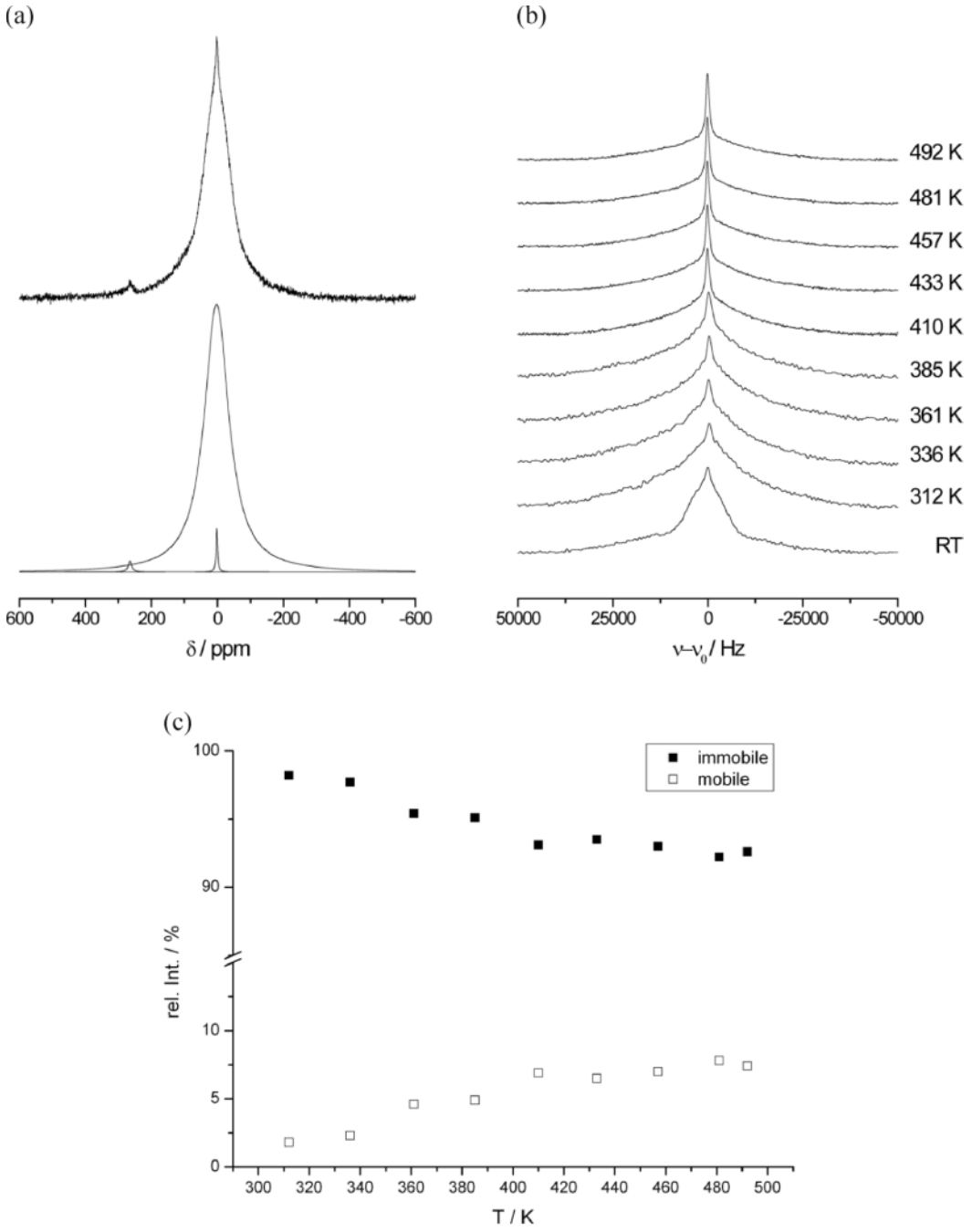

Fig. 5. Static ^{7}Li NMR results on LiBC: (a) experimental (top) and simulated (below) static ^{7}Li NMR spectrum of LiBC at room temperature. Individual lineshape components used in the simulation are indicated. The small peak near 260 ppm is due to a small elemental Li impurity; (b) temperature-dependent static ^{7}Li NMR spectra of LiBC; (c) temperature-dependent fractions of mobile and immobile Li ions in LiBC as determined by peak integration.

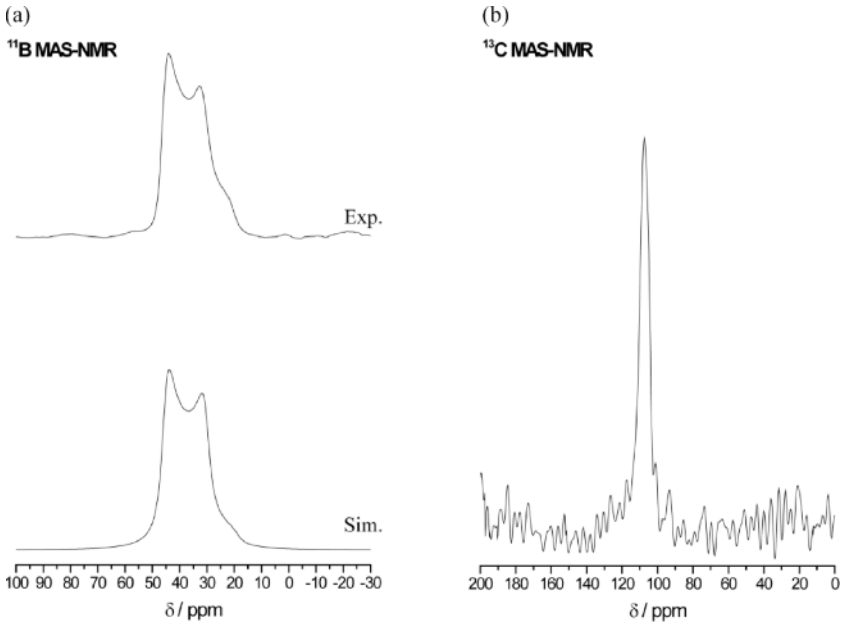

Fig. 6. (a) Experimental and simulated ^{11}B MAS-NMR spectra of LiBC at room temperature and a spinning frequency of 24.0 kHz, measured at 9.4 T; (b) room-temperature ^{13}C MAS-NMR spectrum, measured at 7.05 T and a spinning frequency of 12 kHz.

($C_Q = 3.36$ MHz, $\eta_Q = 0$, $\delta_{iso} = 38$ ppm) [44] and are consistent with the planar BC_3 local environment of the boron species within the [BC] layers. The ^{13}C MAS-NMR spectrum (Fig. 6b) shows a single peak at 107.4 ppm as expected from the crystal structure. Comparable chemical shifts have been reported for the carbon atoms located on the polar sites of the B_4C structure [45], for graphite [46], and for a variety of sp^2-hybridized carbonaceous materials [47]. All of the latter materials, specifically graphite, show substantial MAS-NMR linewidths, generally in excess of 50 ppm, which can be attributed to magnetic susceptibility anisotropy effects [47]. In contrast, the rather small ^{13}C NMR linewidth in Fig. 6b indicates that in LiBC such susceptibility effects are negligible, in agreement with the ionic bonding model proposed for this compound.

Acknowledgement

We thank Dipl.-Ing. U. Ch. Rodewald for collecting the single-crystal diffractometer data. This work was financially supported by the Deutsche Forschungsgemeinschaft (PAK 177) and the Bundesministerium für Forschung und Technologie (LiVe – Lithium-Verbundstrukturen within the program LIB 2015). S. D. acknowledges a personal fellowship from the Fonds der Chemischen Industrie.

[1] J. O. Besenhard, M. Winter, *Pure Appl. Chem.* **1998**, *70*, 603.
[2] M. Winter, J. O. Besenhard, *CHIUZ* **1999**, *33*, 320.
[3] M. Winter, W. K. Appel, B. Evers, T. Hodal, K.-C. Möller, I. Schneider, M. Wachtler, M. R. Wagner, G. H. Wroddnig, J. O. Besenhard, *Monatsh. Chem.* **2001**, *132*, 473.
[4] J. P. Olivier, M. Winter, *J. Power Sources* **2001**, 97 – 98, 151.
[5] T. Placke, V. Siozios, R. Schmitz, S. F. Lux, P. Bieker, C. Colle, H. W. Meyer, S. Passerini, M. Winter, *J. Power Sources* **2012**, *200*, 83.
[6] J. O. Besenhard, M. Winter, *Chem. Phys. Chem.* **2002**, *2*, 155.
[7] K. Tasaki, A. Goldberg, M. Winter, *Electrochim. Acta* **2011**, *56*, 10424.
[8] M. Winter, J. O. Besenhard, M. E. Spahr, P. Novak, *Adv. Mater.* **1998**, *10*, 725.
[9] W. Kohs, H. J. Santner, F. Hofer, H. Schröttner, J. Doninger, I. Barsukov, J. P. Olivier, J. H. Albering, K.-C. Möller, J. O. Besenhard, M. Winter, *J. Power Sources* **2012**, *200*, 83.
[10] M. Wörle, R. Nesper, G. Mair, M. Schwarz, H. G. von Schnering, *Z. Anorg. Allg. Chem.* **1995**, *621*, 1153.

[11] J. Nagmatsu, N. Nakagawa, T. Muranaka, Y. Zenitani, J. Akimitsu, *Nature* **2001**, *21*, 410.
[12] H. Rosner, A. Kitaigorodsky, W. E. Pickett, *Phys. Rev. Lett.* **2002**, *88*, 127001.
[13] A. M. Fogg, J. Meldrum, G. R. Darling, J. B. Claridge, M. J. Rosseinsky, *J. Am. Chem. Soc.* **2006**, *128*, 10043.
[14] L. Zhao, P. Klavins, K. Liu, *J. Appl. Phys.* **2003**, *93*, 8653.
[15] A. Bharathi, S. J. Balaselvi, M. Premila, T. N. Sairam, G. L. N. Reddy, C. S. Sundar, Y. Hariharan, *Solid State Commun.* **2002**, *124*, 423.
[16] A. M. Fogg, P. R. Chalker, J. B. Claridge, G. R. Darling, M. J. Rosseinsky, *Phys. Rev. B* **2003**, *67*, 245106.
[17] A. M. Fogg, J. B. Claridge, G. R. Darling, M. J. Rosseinsky, *Chem. Commun.* **2003**, 1348.
[18] Y. Nakamori, S.-I. Orimo, *J. Alloys Compd.* **2004**, *370*, L7.
[19] B. Renker, H. Schober, P. Adelmann, P. Schweiss, K.-P. Bohnen, R. Heid, *Phys. Rev. B* **2004**, *69*, 052506.
[20] D. Souptel, Z. Hossain, G. Behr, W. Löser, C. Geibel, *Solid State Commun.* **2003**, *125*, 17.
[21] A. V. Pronin, K. Pucher, P. Lunkenheimer, A. Krimmel, A. Loidl, *Phys. Rev. B* **2003**, *67*, 132502.
[22] A. M. Fogg, G. R. Darling, J. B. Claridge, J. Meldrum, M. J. Rosseinsky, *Phil. Trans. R. Soc. London Ser. A* **2008**, 366, 55.
[23] Q. Xu, C. Ban, A. C. Dillon, S.-H. Wei, Y. Zhao, *J. Phys. Chem. Lett.* **2011**, *2*, 1129.
[24] D. Kußmann, R.-D. Hoffmann, R. Pöttgen, *Z. Anorg. Allg. Chem.* **1998**, *624*, 1727.
[25] P. A. Beckmann, C. Dybowski, *J. Magn. Reson.* **2000**, *146*, 379.
[26] D. Massiot, F. Fayon, M. Capron, I. King, S. Le Calvé, B. Alonso, J. O. Durand, B. Bujoli, Z. Gan, G. Hoatson, *Magn. Reson. Chem.*, **2002**, *40*, 70.
[27] G. M. Sheldrick, SHELXL-97, Program for Crystal Structure Refinement, University of Göttingen, Göttingen (Germany) **1997**. See also: G. M. Sheldrick, *Acta Crystallogr.* **2008**, *A64*, 112.
[28] J. W. Nielsen, N. C. Baenziger, *Acta Crystallogr.* **1954**, *7*, 132.
[29] R.-D. Hoffmann, R. Pöttgen, *Z. Kristallogr.* **2001**, *216*, 127.
[30] J. Emsley, *The Elements*, Oxford University Press, Oxford **1999**.
[31] R. Juza, V. Wehle, *Naturwissenschaften* **1965**, *52*, 560.
[32] M. R. Wagner, J. H. Albering, K. C. Möller, J. O. Besenhard, M. Winter, *Electrochem. Commun.* **2005**, *7*, 947.
[33] H. J. Santner, K.-C. Möller, J. Ivanco, M. G. Ramsey, F. P. Netzer, S. Yamaguchi, J. O. Besenhard, M. Winter, *J. Power Sources* **2003**, 119 – 121, 368.
[34] J. O. Besenhard, M. W. Wagner, M. Winter, A. D. Jannakoudakis, P. D. Jannakoudakis, E. Theodoridou, *J. Power Sources* **1993**, *44*, 413.
[35] M. Winter, *Z. Phys. Chem.* **2009**, *223*, 1395.
[36] M. R. Wagner, P. Raimann, K. C. Möller, J. O. Besenhard, M. Winter, *Electrochem. Solid-State Lett.* **2004**, *7*, A201.
[37] M. Winter, H. Buqa, B. Evers, T. Hodal, K. C. Möller, C. Reisinger, M. V. Santis Alvarez, I. Schneider, G. H. Wrodnigg, F. P. Netzer, R. Blyth, M. G. Ramsey, P. Golob, F. Hofer, C. Grogger, W. Kern, R. Saf, J. O. Besenhard, *ITE Battery Lett.* **1999**, *1*, 129.
[38] J. A. Seel, J. R. Dahn, *J. Electrochem. Soc.* **2000**, *147*, 892.
[39] T. Placke, P. Bieker, S. F. Lux, O. Fromm, H.-W. Meyer, S. Passerini, M. Winter, *Z. Phys. Chem.* **2012**, *226*, 391.
[40] T. Placke, O. Fromm, S. F. Lux, P. Bieker, S. Rothermel, H.-W. Meyer, S. Passerini, M. Winter, *J. Electrochem. Soc.*, submitted for publication.
[41] S. E. Hayes, R. A. Guidotti, W. R. Even, P. J. Hughes, H. Eckert, *J. Phys. Chem. A* **2003**, *107*, 3866 and refs. therein.
[42] K. Tatsumi, T. Akai, T. Imamura, K. Zaghib, S. Higuchi, Y. Sawada, *J. Electrochem. Soc.* **1996**, *143*, 1923.
[43] J. Conard, P. Lauginie, *TANSO* **2000**, *191*, 62.
[44] Y. Lee, D. Y. Han, D. Lee, A. J. Wook, S. H. Lee, D. Lee, Y. K. Kim, *Carbon* **2002**, *40*, 403.
[45] F. Mauri, N. Vast, C. J. Picard, *Phys. Rev. Lett.* **2001**, *87*, 85506.
[46] P. Lauginie, A. Messaoudi, J. Conard, *Synth. Met.* **1993**, *55*, 3002.
[47] J. C. C. Freitas, F. G. Emmerich, G. R. C. Cernicchiaro, L. C. Sampaio, T. J. Bonagamba, *Solid State Nucl. Magn. Reson.* **2001**, *20*, 61.